THE JOURNAL OF BIOLOGICAL CHEMISTRY VOL. 285, NO. 6, pp. 3685–3694, February 5, 2010

Comparative Study of the Gating Motif and C-type Inactivation in Prokaryotic Voltage-gated Sodium Channels*

Received for publication, September 10, 2009, and in revised form, December 2, 2009 Published, JBC Papers in Press, December 3, 2009, DOI 10.1074/jbc.M109.057455

Katsumasa Irie[‡§], Kazuya Kitagawa[‡], Hitoshi Nagura[‡1], Tomoya Imai[¶], Takushi Shimomura[‡], and Yoshinori Fujiyoshi[‡2]

From the [‡]Department of Biophysics, Graduate School of Science, Kyoto University, Oiwake, Kitashirakawa, Sakyo-ku, Kyoto 606-8502, the [§]Japan Biological Informatics Consortium, Oiwake, Kitashirakawa, Sakyo-ku, Kyoto 606-8502, and the [¶]Research Institute for Sustainable Humanosphere (RISH), Kyoto University, Gokasho, Uji, Kyoto 611-0011, Japan

Prokaryotic voltage-gated sodium channels (Na_Vs) are homotetramers and are thought to inactivate through a single mechanism, named C-type inactivation. Here we report the voltage dependence and inactivation rate of the NaChBac channel from *Bacillus halodurans*, the first identified prokaryotic Na_V, as well as of three new homologues cloned from *Bacillus licheniformis* (Na_VBacL), *Shewanella putrefaciens* (Na_VSheP), and *Roseobacter denitrificans* (Na_VRosD). We found that, although activated by a lower membrane potential, Na_VBacL inactivates as slowly as NaChBac. Na_VSheP and Na_VRosD inactivate faster than NaChBac. Mutational analysis of helix S6 showed that residues corresponding to the "glycine hinge" and "P*X*P motif" in voltage-gated potassium channels are not obligatory for channel gating in these prokaryotic Na_Vs, but mutations in the regions changed the inactivation rates. Mutation of the region corresponding to the glycine hinge in Na_VBacL (A214G), Na_VSheP (A216G), and NaChBac (G219A) accelerated inactivation in these channels, whereas mutation of glycine to alanine in the lower part of helix S6 in NaChBac (G229A), Na_VBacL (G224A), and Na_VRosD (G217A) reduced the inactivation rate. These results imply that activation gating in prokaryotic Na_Vs does not require gating motifs and that the residues of helix S6 affect C-type inactivation rates in these channels.

Voltage-gated sodium channels (Na_Vs)[3] generate the rapid upstroke of action potentials in nerve cell axons (1). In mammalian Na_Vs, the channel is formed by the α-subunit, which comprises four repeats of six-transmembrane segments, with each repeat consisting of 300–400 amino acids. The α-subunit carries several glycosylation sites and co-assembles with auxiliary subunits to form the native channel (2, 3). The only structural information on Na_Vs available to date is a density map of the Na_V from the electric organ of the electric eel determined by cryoelectron microscopy (4). Due to its limited resolution of 19 Å, the density map did not provide insights into the gating or sodium selectivity.

The first prokaryotic Na_V, NaChBac, was cloned from *Bacillus halodurans* (5). Subsequently, three more prokaryotic sodium channels were cloned and characterized (6, 7). All studied prokaryotic Na_Vs form homotetramers with a structure thought to be similar to that of some potassium channels with known structures (8–10). Furthermore, because the proteins could be expressed in large amounts in *Escherichia coli* and purified by metal chelate affinity chromatography (5, 7, 11), they are promising candidates for high resolution structure determination and structure-function analyses.

The physiological role of prokaryotic Na_Vs may be related to pH homeostasis, motility, and chemotaxis (6, 12). Searching bacterial genomic data bases, we found 26 sequences of putative NaChBac homologues from bacteria living in various environments. We were able to clone the putative Na_V genes from three of these bacteria, *Bacillus licheniformis*, *Shewanella putrefaciens*, and *Roseobacter denitrificans*, and named them Na_VBacL, Na_VSheP, and Na_VRosD, respectively. These homologues showed unique channel properties optimized for the specific environments in which the bacteria live.

We found an unexpected feature in the primary structure of Na_VSheP, namely a lack of glycine residues in helix S6. Crystal structures of potassium channels revealed that glycine and proline residues in helix S6 that are part of the "glycine hinge" and "P*X*P motif," respectively, create kinks in the open state (13–15). It has therefore been thought that these residues are critical for activation gating in tetrameric cation channels (15–19). Although Na_VSheP contains no glycine residues in helix S6, it still shows typical inward currents. To better understand their role, we mutated the glycine residues in helix S6 of Na_VBacL, Na_VRosD, and NaChBac to alanine. All mutants retained inward sodium currents. These results suggest that the previously proposed gating motifs are not obligatory for activation of prokaryotic Na_Vs.

The glycine mutations had no effect on activation but affected inactivation of the channels. Generally, voltage-gated cation channels are immediately inactivated after activation. Tetrameric cation channels have mainly two inactivation mechanisms, N-type and C-type inactivation (20–25). N-type

* This work was supported in part by Grants-in-Aid for Specially Promoted Research and the Japan New Energy and Industrial Technology Development Organization.

The nucleotide sequence(s) reported in this paper has been submitted to the DDBJ/GenBank™/EBI Data Bank with accession number(s) AB517991, AB517992, and AB517993.

[1] Supported by a fellowship from the Japan Society for the Promotion of Science.

[2] To whom correspondence should be addressed: Dept. of Biophysics, Graduate School of Science, Kyoto University, Oiwake, Kitashirakawa, Sakyo-ku, Kyoto 606-8502, Japan. Tel.: 81-75-753-4216; Fax: 81-75-753-4218; E-mail: yoshi@em.biophys.kyoto-u.ac.jp.

[3] The abbreviations used are: Na_V, voltage-gated sodium channel; K_V, voltage-gated potassium channel; MALDI, matrix-assisted laser desorption ionization; TOF, time-of-flight; CHO, Chinese hamster ovary; HEK, human embryonic kidney.

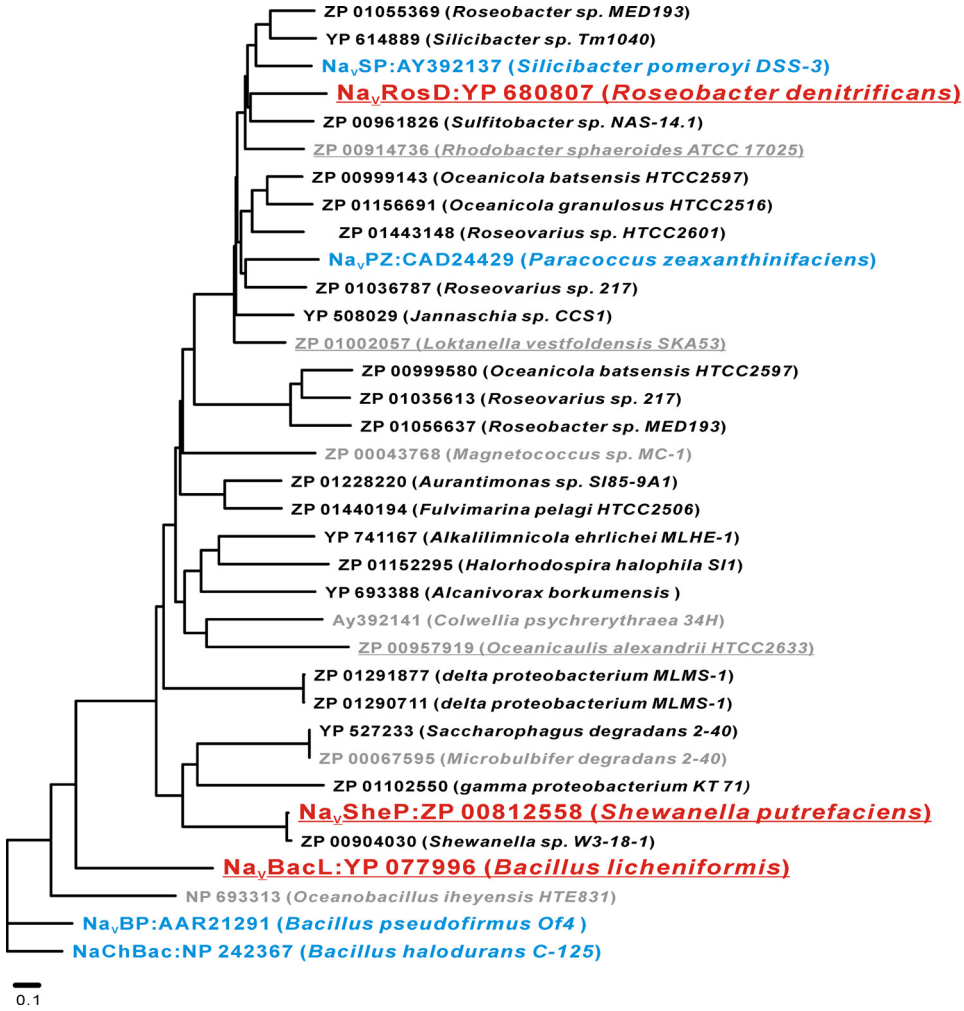

FIGURE 1. **Phylogenetic tree of bacterial NaChBac homologues.** A phylogenetic tree shows the bacterial species that express NaChBac homologues and their GenBank™ accession numbers. The program ClustalW was used to calculate a multiple sequence alignment based on conserved sequences of the NaChBac homologues. The phylogenetic tree was generated using the program PROTDIST, part of the PHYLIP package (Phylogeny Inference Package; available on the World Wide Web). The branch lengths are proportional to the sequence divergence, with the *scale bar* corresponding to 0.1 substitution per amino acid site. *Red underlined*, homologues that were newly cloned and functionally characterized in this study; *gray underlined*, homologues that could not be cloned in this study; *blue*, homologues that were functionally characterized previously; *gray*, homologues that were previously cloned but did not show detectable channel activity.

or fast inactivation is thought to be mediated by the interdomain linkers of Na_Vs or the N termini of voltage-gated potassium channels, a mechanism described by the "ball and chain" model (20–22). Although C-type inactivation is common in tetrameric cation channels, its molecular mechanism remains unclear. It has been proposed that C-type inactivation may be related to a collapse of the selectivity filter (23–25). Prokaryotic Na_Vs lack an obvious cytoplasmic N-type inactivation peptide, and inactivation may thus only occur through the C-type inactivation mechanism (25, 26). Furthermore, comparative studies and mutational analysis of these new Na_V homologues provide evidence that the rate of C-type inactivation is affected by the residues of helix S6.

EXPERIMENTAL PROCEDURES

Cloning of NaChBacs Homologues and Site-directed Mutagenesis—The NaChBac amino acid sequence (NP_242367) was used as a query for a BLASTP search against the Microbial Genomic data base at NCBI. The identified primary sequence data were obtained from Entrez at NCBI (*B. licheniformis* ATCC 14580 DSM 13 as NC_006270, *Loktanella vestfoldensis* SKA53 as NZ_AAMS01000001, *Rhodobacter sphaeroides* ATCC 17025 as NZ_AAME01000021, *S. putrefaciens* CN-32 as NZ_AALB00000000, *R. denitrificans* OCh 114 as NC_008209, and *Oceanicaulis alexandrii* HTCC2633 as NZ_AAMQ01000008). Samples of *B. licheniformis* (Japan Collection of Microorganisms number 2505), *L. vestfoldensis* (Japan Collection of Microorganisms number 21637) and *R. sphaeroides* (Japan Collection of Microorganisms number 6121) were obtained from the RIKEN BioResource Center. Samples of *S. putrefaciens* (National Institute of Technology and Evaluation Biological Resource Center number 3908), *R. denitrificans* (National Institute of Technology and Evaluation Biological Resource Center number 15277), and *Oceanicaulis* sp. (National Institute of Technology and Evaluation Biological Resource Center number 101722), closely related to O. *alexandrii* by 16 S rRNA sequence analysis, were obtained from the National Institute of Technology and Evaluation. DNAs of NaChBac homologues were directly cloned by PCR from colonies of bacteria using PrimeSTAR® GXL DNA Polymerase (Takara Bio.).

The following primers were used for cloning: 5′-CGCGGATCCATGAACACTCATCAAAATCGA-3′ and 5′-CGCGGATCCATCTTTCTTTTCATTTTGGGT-3′ for *B. licheniformis*; 5′-CGCGGATCCATGAGTACATCTTTACTT-3′ and 5′-CGCGGATCCGTCAGAACCAATGTTTCC-3′ for *S. putrefaciens*; 5′-CGCGGATCCATGGGTGTAAGAGAGCAA-3′ and 5′-CGCGGATCCGGACCGGGGCCTGTCTTT-3′ for *R. denitrificans*; 5′-CGCGGATCCATGAATTTGCGCGCCAGAACA-3′ and 5′-CGCGGATCCCTTGCCCGCCTGATCCAGTCG-3′ for *L. vestfoldensis*; 5′-CGCGGATCCATGACAGTGCGGGAAATGGTA-3′ and 5′-CGCGGATCCGCCGCGCGTCTCGTCGCCCGC-3′ for *R. sphaeroides*; and 5′-CGCGGATCCATGAGCGACGCGTCGGCC-3′ and 5′-CGCGGATCCCTCGGAATTGTCCGCCCG-3′ for *O. alexandrii*.

PCR products were cloned into a modified pET21b plasmid (Novagen) using BamHI restriction sites. These cloned DNAs contained additional methionine, glycine, and serine codons

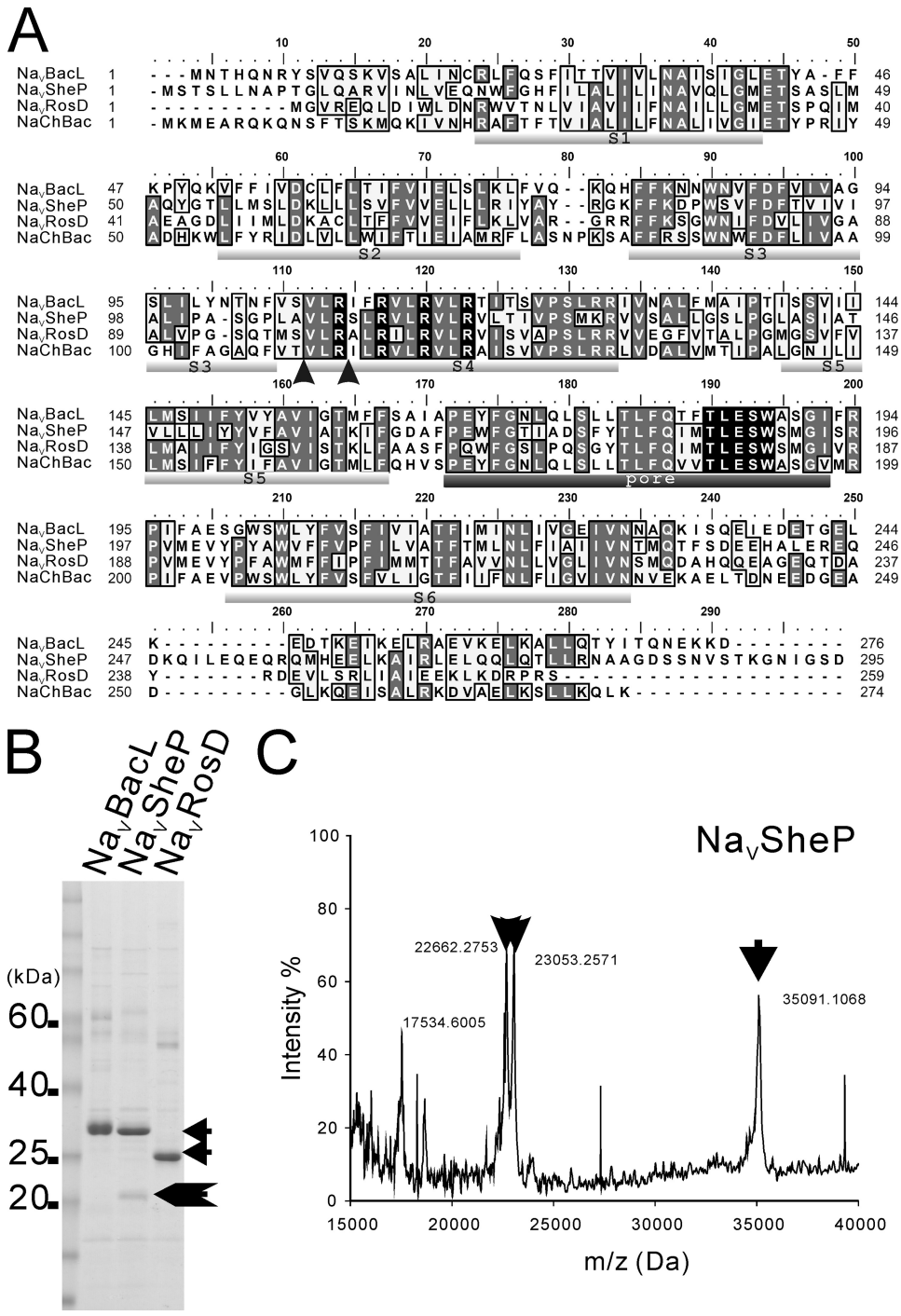

FIGURE 2. **Primary structures and expression of NaChBac homologues.** *A*, alignment of the deduced amino acid sequences of Na_VBacL, Na_VSheP, Na_VRosD, and NaChBac. The six putative transmembrane domains (S1–S6) are *underlined* in *light gray*, and the putative pore region is *underlined* in *dark gray*. Conserved arginines in helix S4 implicated in voltage sensing and residues constituting the putative sodium selectivity filter are shown as *white letters* in *black boxes*. The *arrowheads* indicate cleavage sites in Na_VSheP identified by MALDI mass spectrometry. *B*, Coomassie-stained SDS-PAGE of Na_VBacL, Na_VSheP, and Na_VRosD purified by Co^{2+} affinity chromatography. *C*, MALDI-TOF peptide mass spectrum of purified Na_VSheP. The *x* axis represents the mass-to-charge ratio (*m/z*), and the *y* axis represents relative abundance. The *arrow* indicates the full-length NaChBac homologues, and the *arrowheads* indicate fragments of Na_VSheP.

before the first methionine and a thrombin cleavage site before the C-terminal His tag. For expression in mammalian cells, three NaChBac homologues (Na_VBacL from *B. licheniformis*, Na_VSheP from *S. putrefaciens*, and Na_VRosD from *R. denitrificans*) were subcloned into the pCI vector (Promega) using the NheI and KpnI sites. Site-directed mutagenesis was accomplished by PCR of the full-length pCI plasmid containing the Na_V gene using high fidelity *Pfu* DNA polymerase (method by Stratagene). All clones were confirmed by DNA sequencing.

Expression and Purification of Recombinant Prokaryotic Na_Vs—Proteins were expressed in *E. coli* BL21 Δstar™ (DE3) (Invitrogen). 100 ml of LB medium (Invitrogen) containing 100 μg/ml ampicillin (Wako) was inoculated with 10 μl of glycerol stock and incubated overnight at 37 °C. 12.5 ml of the saturated culture medium was then used to inoculate 1.25 liters of LB medium containing 40 μg/ml ampicillin, and cells were grown at 37 °C to an A_{600} of 0.8. Cells were induced with 0.5 mM isopropyl 1-thio-β-D-galactopyranoside (Wako) and grown for 16 h at 18 °C. Cells were suspended in TBS buffer (20 mM Tris-HCl, pH 7.4, 300 mM NaCl) and lysed using a French press (SLM AMINCO) at 12,000 p.s.i. Membranes were collected by centrifugation (100,000 × *g*, 1 h, 4 °C) and solubilized by homogenization in TBS buffer containing 40 mM CYMAL-5 (Anatrace). After centrifugation (40,000 × *g*, 30 min, 4 °C), the supernatant was loaded onto a HIS-Select® cobalt affinity gel column (Sigma). The column was washed with 10 mM imidazole in TBS buffer containing 8 mM CYMAL-5, and the protein was eluted with 300 mM imidazole. Purified proteins were resolved on 10–20% SDS-PAGE gradient gels (Wako) and stained with Coomassie Blue. The BenchMark™ prestained protein ladder (Invitrogen) was used as molecular weight markers.

Mass Spectrometry—Mass spectrometry was carried out with a MALDI-TOF instrument (Voyager-DE, Applied Biosystems), using α-cyanohydroxycinnamic acid (Sigma) as matrix. Protein samples were mixed with the same volume of 90% acetonitrile (Wako) and 0.2% trifluoroacetic acid (Sigma), loaded onto a sample plate, dried, and washed with deionized water. Finally, 1% α-cyanohydroxycinnamic acid dissolved in 50% acetonitrile and 0.1% trifluoroacetic acid was

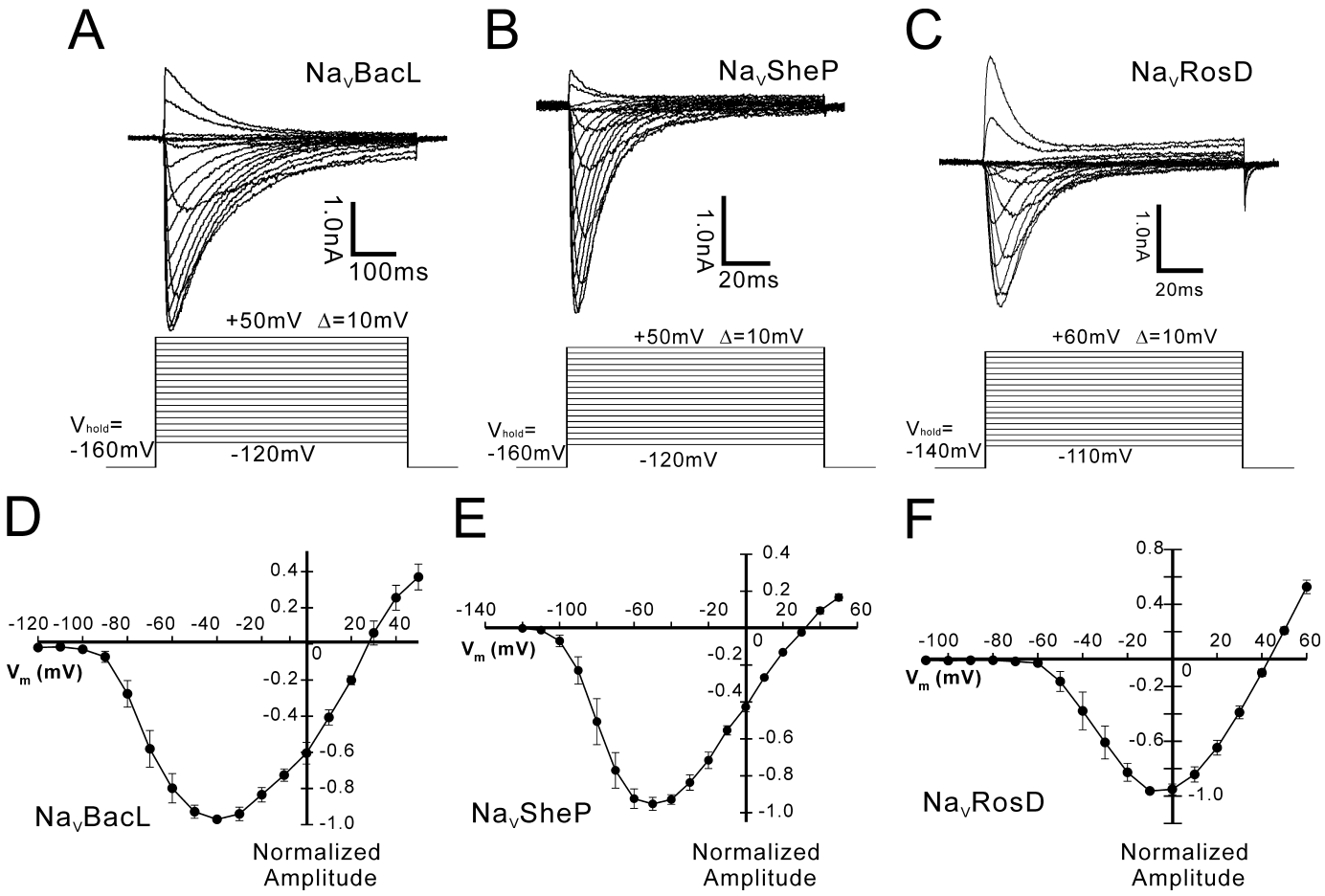

FIGURE 3. **Functional expression of Na_VBacL, Na_VSheP, and Na_VRosD in HEK 293 cells.** *A–C*, representative traces of $I_{NaVBacL}$, $I_{NaVSheP}$, and $I_{NaVRosD}$ resulting from the voltage protocol shown *below* (*D–F*). Averaged ($n = 7$; ±S.E.) peak current-voltage (*I/V*) relation of Na_VBacL, Na_VSheP, and Na_VRosD normalized by the peak current. V_{Hold} indicates the holding potential. The intersweep interval was 15 s.

loaded onto the dried samples. Mass spectra were collected using the delayed extraction mode.

Mammalian Electrophysiology—Chinese hamster ovary (CHO)-K1 or human embryonic kidney (HEK) 293 cells were grown in Dulbecco's modified Eagle's medium (Sigma) complemented with 10% fetal bovine serum (BioWhittaker), 100 units/ml penicillin (Invitrogen), and 100 μg/ml streptomycin (Invitrogen) at 37 °C under 5% CO_2. Cells were transfected with Na_V and pEGFP DNA using the calcium phosphate transfection kit (Invitrogen) and plated onto coverslips. Currents were recorded 12 h (Na_VBacL and Na_VSheP) or 36 h (Na_VRosD and NaChBac) after transfection. The pipette solution contained 105 mM CsF, 35 mM NaCl, 10 mM EGTA, and 10 mM HEPES (pH 7.4). The bath solution contained 150 mM NaCl, 1.5 mM $CaCl_2$, 1 mM $MgCl_2$, 2 mM KCl, 10 mM HEPES (pH 7.4), and 10 mM glucose. For measurements of the voltage dependence of Na_VBacL and Na_VSheP, 150 mM NaCl in the bath solution was replaced by 75 mM NaCl and 75 mM *N*-methyl-D-glucamine. All experiments were conducted at 25 ± 2 °C. Nifedipine (Sigma) was dissolved in DMSO (Wako). The final concentration of the solvent was less than 1%. Whole-cell patch clamp recordings of wild-type NaChBac confirmed that 1% DMSO did not affect the channel activity. All chemicals were dissolved in water. All other compounds were applied to the cultured cells using a perfusion system. For pharmacological measurements, cells were perfused with bath solution containing the inhibitors for 5 min prior to recording currents. All results are presented as mean ± S.E. A simple comparison between Na_VBacL wild type and G201A was made by Student's *t* test. To assess statistical differences in time constants between wild type and mutant proteins, multiple comparisons were made by one-way analysis of variance followed by the Tukey-Kramer multiple comparisons test.

RESULTS

We used the full NaChBac sequence for a standard BLASTP search against the GenBank™ data base of prokaryotic genomic sequences. The BLASTP search yielded 34 sequences that contained both a "TLESW" sequence, the putative selectivity filter of prokaryotic sodium channels (5–7), and positively charged amino acids at every third position in helix S4, the hallmark of voltage sensors (3, 5) (Fig. 1). The channel activity of four of the identified homologues (NaChBac as NP242367, Na_VBP as AAR21291, Na_VPZ as CAD24429, and Na_VSP as AY392137) had already been established (5–7), whereas four other homologues (NP 693313 of *Oceanobacillus iheyensis* HTE831, ZP 00067595 of *Microbulbifer degradans* 2-40, Ay392141 of *Colwellia psychrerythraea* 34H, and ZP 00043768 of *Magnetococcus* sp. *MC-1*) showed no channel activity in previous studies (7). Of the bacteria containing the remaining 26

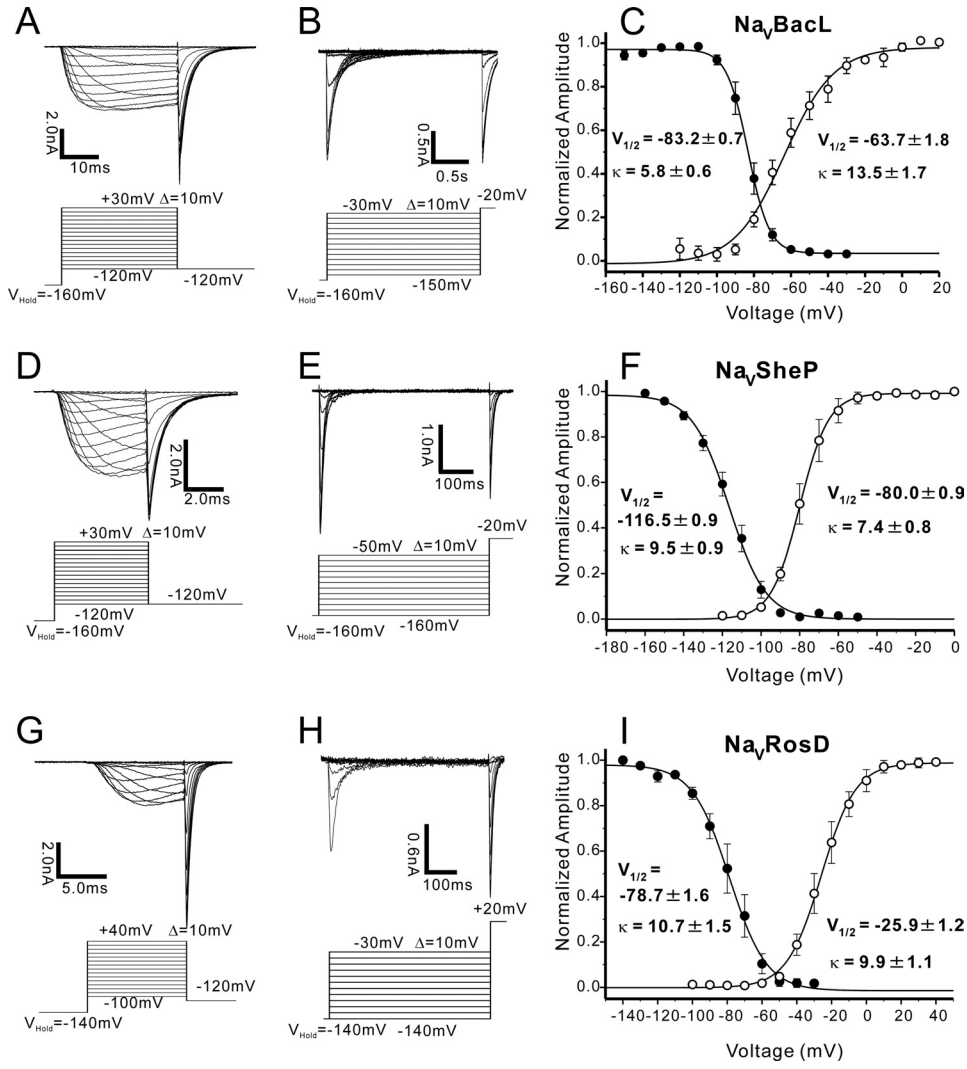

FIGURE 4. **Voltage-dependent activation and inactivation of Na_VBacL, Na_VSheP, and Na_VRosD.** *A*, $I_{NaVBacL}$ deactivation tail currents. After prepulses of varying depolarization (from −120 to +30 mV, increments of +10 mV), tail currents were measured at −120 mV. *B*, $I_{NaVBacL}$ steady-state inactivation currents. After a 2-s prepulse, the channels inactivated to a steady-state level and were reactivated by a second depolarizing pulse (−20 mV). *C*, $I_{NaVBacL}$-normalized activation curve (*open circle*, $n = 9$; ±S.E.) and steady-state inactivation curve (closed circle, $n = 9$; ±S.E.). *D*, $I_{NaVSheP}$ deactivation tail currents. After prepulses of varying depolarization (from −120 to +30 mV, increments of +10 mV), tail currents were measured at −120 mV. *E*, $I_{NaVSheP}$ steady-state inactivation currents. After a 500-ms prepulse, the channels inactivated to a steady-state level and were reactivated by a second depolarizing pulse (−20 mV). *F*, $I_{NaVSheP}$-normalized activation curve (*open circle*, $n = 6$; ±S.E.) and steady-state inactivation curve (*closed circle*, $n = 6$; ±S.E.). *G*, $I_{NaVRosD}$ deactivation tail currents. After prepulses of varying depolarization (from −100 to +40 mV, increments of +10 mV), tail currents were measured at −120 mV. *H*, $I_{NaVRosD}$ steady-state inactivation currents. After a 500-ms prepulse, the channels inactivated to a steady-state level and were reactivated by a second depolarizing pulse (+20 mV). *I*, $I_{NaVRosD}$-normalized activation curve (*open circle*, $n = 6$; ±S.E.) and steady-state inactivation curve (*closed circle*, $n = 6$; ±S.E.). The voltages with half-inactivation/activation and the slope factors are indicated as $V_{1/2}$ (mV) and κ (mV/e-fold), respectively in *C*, *F*, and *I*. The intersweep interval was 15 s in *A*, *B*, *D*, *E*, *G*, and *H*.

homologues, six of them were commercially available: *B. licheniformis*, isolated from soil and plant material (27), and *L. vestfoldensis* (28), *R. sphaeroides* (29), *S. putrefaciens* (30), *R. denitrificans* (31), and *Oceanicaulis* sp. (32) isolated from sea water (28–33). Using the colony-direct PCR method, we were able to clone the putative Na_V genes from three of these six bacteria, namely from *B. licheniformis*, *S. putrefaciens*, and *R. denitrificans*.

Sequencing of the Na_VBacL gene from *B. licheniformis* revealed an open reading frame of 276 amino acids with a predicted molecular size of 31.8 kDa, and sequencing of the Na_VRosD gene from *R. denitrificans* showed an open reading frame of 259 amino acids (29.2 kDa). Both sequences were identical with the deposited sequences. Our sequence of the Na_VSheP gene from *S. putrefaciens*, encoding an open reading frame of 295 amino acids (33.1 kDa), differed, however, from the sequence deposited in the GenBank™ data base in several places (T31A, A54T, V62L, and N88S) (Fig. 2*A*). Na_VBacL, Na_VSheP, and Na_VRosD share with NaChBac sequence identities (sequence similarities) of 49% (57%), 32% (44%), and 37% (48%), respectively, and hydropathy plots predict a six-transmembrane architecture for all three proteins (Fig. 2*A*).

C-terminally His-tagged constructs of all three Na_Vs expressed well in *E. coli* and could be purified by metal chelate affinity chromatography (Fig. 2*B*). Na_VBacL and Na_VRosD migrated as a single band on SDS-polyacrylamide gels (~34 and ~25 kDa, respectively), whereas Na_VSheP migrated mainly as a ~35 kDa band but also showed additional smaller bands. The smaller bands could also be detected on Western blots probed with anti-His antibodies (data not shown). Mass spectra confirmed that all main bands represented the full-length proteins and identified the molecular masses of the smaller bands of Na_VSheP as 22,662 and 23,053 Da (Fig. 2*C*). The additional bands thus represent C-terminal fragments of Na_VSheP that were generated by cleavage of the carboxyl group of residues Arg^{110}, the first arginine of helix S4, and Ala^{107} (Fig. 2*A*).

We transfected mammalian cell lines (CHO-K1 or HEK 293) with the genes encoding Na_VBacL, Na_VSheP, and Na_VRosD and measured the resulting currents (Fig. 3). Although no currents were observed in non-transfected or mock-transfected cells (data not shown), currents could be recorded from cells transfected with the Na_V genes, and all three channels required at least 1 s for 90% recovery from inactivation. Cells transfected with each of the three Na_Vs exhibited large voltage-activated inward currents of up to 10 nA (Fig. 3, *A–C*), peaking at −40, −50, and −10 mV for Na_VBacL, Na_VSheP, and Na_VRosD, respectively (Fig. 3, *D–F*). The reversal potential of Na_VRosD-mediated current ($I_{NaVRosD}$) was

+42.7 mV in a bath solution containing 150 mM Na^+. The inward currents produced by Na_VBacL and Na_VSheP in a bath solution containing 150 mM Na^+ were, however, peaking at a membrane potential that was too low to clamp the membrane potentials at low voltage. To measure the currents produced by Na_VBacL and Na_VSheP, we therefore reduced the NaCl concentration in the bath solution from 150 to 75 mM and added instead 75 mM *N*-methyl-D-glucamine. The reversal potential of $I_{NaVBacL}$ and $I_{NaVSheP}$ could then be determined as +28.3 and +33.0 mV, respectively. Ion substitution (Ca^{2+}, K^+, and *N*-methyl-D-glucamine replacement) confirmed that all three proteins form Na^+-selective channels and that they are sensitive to high concentrations of nifedipine (30 μM) (data not shown). Their pharmacological sensitivity closely resembles that of L-type Ca_Vs, as already reported for the previously characterized homologues (5–7).

$I_{NaVBacL}$ was activated with a time constant ($\tau_{activation}$) of 4.92 ± 0.73 ms at +10 mV (n = 15) and inactivated with $\tau_{inactivation}$ of 96.1 ± 9.60 ms at +10 mV (n = 15). Both time constants were significantly larger than those of mammalian Na_V channels ($\tau_{activation}$ = 2 ms; $\tau_{inactivation}$ = 10 ms) but faster than those of $I_{NaChBac}$ ($\tau_{activation}$ = 12.9 ms; $\tau_{inactivation}$ = 166 ms) (5). $I_{NaVSheP}$ ($\tau_{activation}$ = 0.89 ± 0.076 ms at −10 mV, n = 17; $\tau_{inactivation}$ = 9.90 ± 0.57 ms at −10 mV, n = 17) and $I_{NaVRosD}$ ($\tau_{activation}$ = 1.61 ± 0.12 ms at +20 mV, n = 15; $\tau_{inactivation}$ = 9.88 ± 1.25 ms at +20 mV, n = 15) were activated and inactivated significantly faster than $I_{NaVBacL}$ and $I_{NaChBac}$. Remarkably, the time constants of them were as small as those of the α-subunit of the rat skeletal muscle-type Na_V (34).

We evaluated the voltage-dependent activation of Na_VBacL by measuring deactivation tail currents (Fig. 4*A*). A Boltzmann fit of the averaged activation curve yielded an activating potential of 50% activation ($V_{½}$) of −63.7 ± 1.8 mV (n = 9) and a slope factor (κ) of 13.5 ± 1.7 mV/e-fold change in current (Fig. 4*C*). The steady-state inactivation of the channel was determined by sequential depolarization to test voltages, followed by voltage clamp to the peak of activation at −20 mV (Fig. 4*B*). Steady-state inactivation was a steep function of voltage, with 50% inactivation at −83.2 ± 0.7 mV (n = 9) and κ = 5.8 ± 0.6 mV/e-fold change (Fig. 4*C*). Although Na_VBacL had similar time constants of activation and inactivation as NaChBac (5), Na_VBacL activated and inactivated at voltages about 40 mV lower than those of NaChBac (Table 1).

Boltzmann fits of their activation curves yielded $V_{½}$ of −80.0 ± 0.9 mV and κ of 7.4 ± 0.8 mV/e-fold change for Na_VSheP (n = 6; Fig. 4, *D* and *F*) and $V_{½}$ of −25.9 ± 1.2 mV and κ of 9.9 ± 1.1 mV/e-fold change for Na_VRosD (n = 6; Fig. 4, *G* and *I*). The steady-state inactivation of Na_VSheP and Na_VRosD were dependent on the voltage with half-inactivations at −116.5 ± 0.9 mV (κ = 9.5 ± 0.9 mV/e-fold) (n = 6; Fig. 4, *E* and *F*) and −78.7 ± 1.6 mV (κ = 10.7 ± 1.6 mV/e-fold) (n = 6; Fig. 4, *H* and *I*), respectively. Na_VSheP activated and inactivated at the lowest membrane potential of all NaChBac homologues studied to date. The voltage dependences of the three prokaryotic Na_Vs analyzed in this study are summarized in Table 1.

Previous studies indicated that a glycine residue in the middle of helix S6, named the "glycine hinge," is critical for gating of tetrameric cation channels (15–17). A glycine residue corresponding to the glycine hinge is present in NaChBac (Gly^{219}) but not in Na_VBacL (Ala^{214}), Na_VSheP (Ala^{216}), and Na_VRosD (Thr^{207}) (*red arrow* in Fig. 5*A*). Other glycine residues in Na_VBacL (Gly^{224}), Na_VRosD (Gly^{217}), and also NaChBac (Gly^{229}) are found in the lower part of helix S6. This part is near the cytoplasmic side and corresponds to the position of the P*X*P motif, a Pro-*X*-Pro or glycine motif that is important for gating in hERG (human ether-a-go-go related gene) and K_V channels (18, 19) (*green arrow* in Fig. 5*A*) and creates a kink in helix S6 of K_V1.2 (Fig. 5*C*). By contrast, Na_VSheP contains no glycine residues in helix S6 (Fig. 5*A*).

To evaluate their role, we mutated the glycines in helix S6 of Na_VBacL, Na_VRosD, and NaChBac to alanine, a residue known to strongly stabilize α-helical secondary structure (35). All mutants retained the channel currents, but their time constants of inactivation changed significantly. On the other hand, their activation rates and also voltage dependences were less influenced by the mutations. Table 2 summarizes the $\tau_{activation}$ and $\tau_{inactivation}$ values of all analyzed mutant and wild-type channels as well as the statistical differences in $\tau_{inactivation}$ between the wild-type channels and the various mutants. As a control, we made an alanine substitution of residue Gly^{201} in Na_VBacL, which is located in the pore-S6 loop (*blue arrow* in Fig. 5*A*). This mutation had no effect on the time constant of inactivation (Table 2). With $\tau_{inactivation}$ of 21.4 ± 2.19 ms at +10 mV, the NaChBac G219A mutant showed faster inactivation than wild-type NaChBac ($p < 0.01$) (Fig. 5*D*). NaChBac G229A ($\tau_{inactivation}$ = 230 ± 33.8 ms at +10 mV), Na_VBacL G224A ($\tau_{inactivation}$ = 270 ± 53.3 ms at +10 mV), and Na_VRosD G217A ($\tau_{inactivation}$ = 60.9 ± 13.0 ms at +20 mV) showed significantly slower inactivation than the corresponding wild-type channels ($p < 0.01$) (Fig. 5, *D–F*). Inactivation of the NaChBac G219A/G229A double mutant ($\tau_{inactivation}$ = 156 ± 16.2 ms at +10 mV) showed no statistically relevant difference compared with the inactivation of the wild-type protein and was significantly slower than that of NaChBac G219A (Fig. 5*D*). All mutants lacking glycine residues in helix S6 still showed activation and inactivation.

Na_VBacL, Na_VSheP, and Na_VRosD do not have a glycine at the position that corresponds to the glycine hinge in helix S6. When the residues in this position were mutated to glycine, the mutants, with the exception of Na_VRosD T207G (see below), also produced measurable inward currents (more than 1 nA) (Fig. 5,

TABLE 1

$V_{½}$ of inactivation and activation of prokaryotic Na_Vs

$V_{½}$ of inactivation is the membrane potential of 50% steady-state inactivation. $V_{½}$ of activation is the potential of 50% activation. All results are expressed as mean ± S.E. All experiments were performed at pH 7.4 except for the indicated experiment at pH 9.0.

	$V_{½}$		Note
	Inactivation	Activation	
	mV		
Na_VBacL	−83.2 ± 0.7	−63.7 ± 1.8	n = 9
Na_VSheP	−116 ± 0.9	−80.0 ± 0.9	n = 6
Na_VRosD	−78.7 ± 1.6	−25.9 ± 1.2	n = 6
NaChBac	−40	−24	Ref. 5
Na_VPZ	−35	−10	Ref. 7
Na_VSP	−22	21	Ref. 7
Na_VBP	−57	−35	Ref. 6
	−86	−64	At pH 9.0

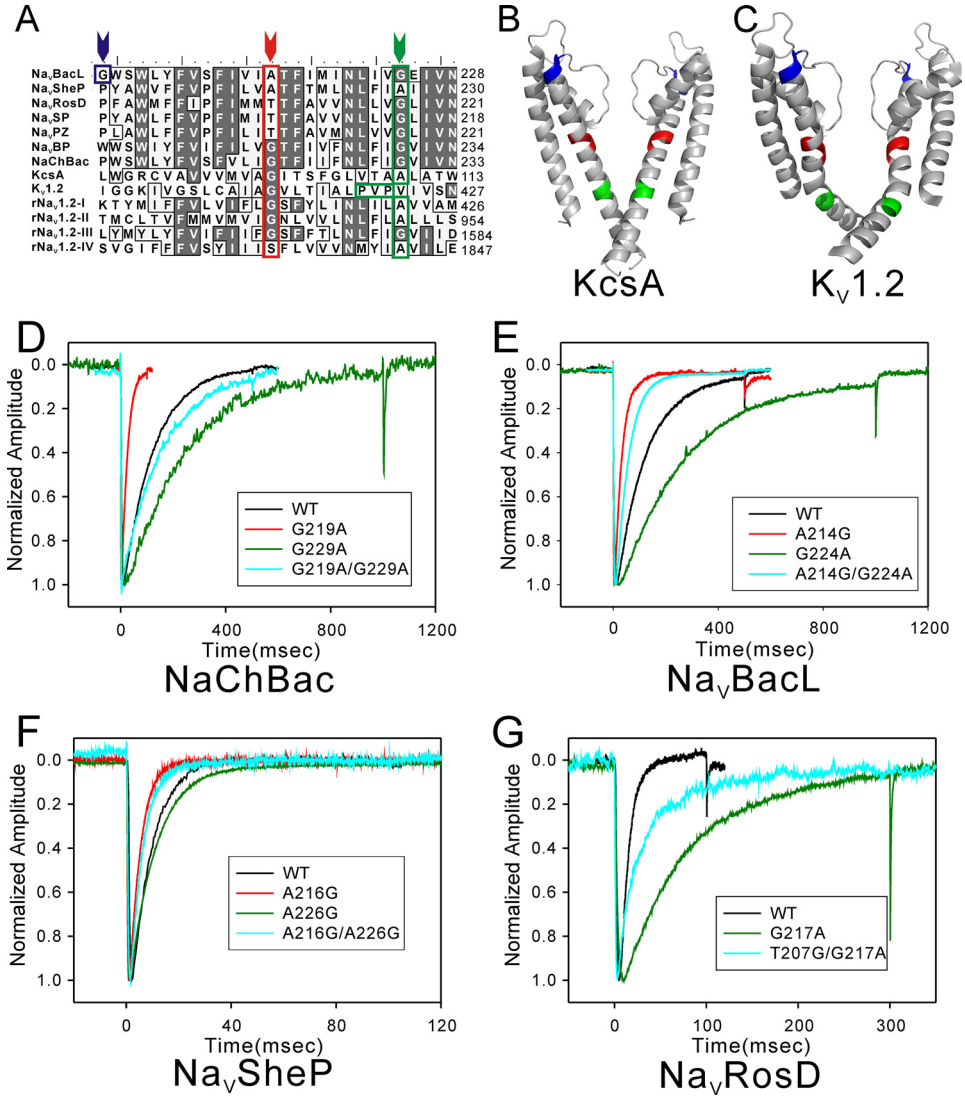

FIGURE 5. **Electrophysiological analysis of the effects of mutations in helix S6.** *A*, alignment of helix S6 and inner helix sequences of Na_VBacL, Na_VSheP, Na_VRosD, Na_VSP, Na_VPZ, Na_VBP, NaChBac, KcsA (potassium channel from *Streptomyces lividans*), K_V1.2 (potassium channel from *Rattus norvegicus*), and the four subdomains (I–IV) of Na_V1.2 (voltage-gated sodium channel from rat brain). The *arrowheads* indicate the positions of G201 in Na_VBacL (*blue*), the glycine hinge (*red*), and the P*X*P motif (*green*); residues of these motifs are *boxed* in the corresponding *colors*. *B* and *C*, *ribbon diagrams* of KcsA (Protein Data Bank code 1r3j) (*B*) and K_V1.2 (Protein Data Bank code 2r9r) (*C*) with the residues and motifs described in *A* shown in the same *colors*. *D*, representative traces of currents produced by wild-type and mutant NaChBac channels activated by the following voltage protocol. After holding the potential at −120 mV, currents were measured at +10 mV for 500 ms (wild type (*WT*) and G219A/G229A), 100 ms (G219A), and 1 s (G229A). *E*, representative traces of currents produced by wild-type and mutant Na_VBacL channels activated by the following voltage protocol. After holding the potential at −160 mV, currents were measured at +10 mV for 500 ms (wild type, A214G, and A214G/G224A) and 1 s (G224A). *F*, representative traces of currents produced by wild-type and mutant Na_VSheP channels activated by the following voltage protocol. After holding the potential at −160 mV, currents were measured at −10 mV for 100 ms. *G*, representative traces of currents produced by wild-type and mutant Na_VRosD channels activated by the following voltage protocol. After holding the potential at −140 mV, currents were measured at +20 mV for 100 ms (wild type) and 300 ms (G217A and T207G/G217A).

D–F). Furthermore, Na_VBacL A214G ($\tau_{inactivation}$ = 29.5 ± 3.14 ms at +10 mV) and Na_VSheP A216G ($\tau_{inactivation}$ = 5.35 ± 0.72 ms at −10 mV) showed significantly faster inactivation than the respective wild-type channels ($p < 0.01$) (Fig. 5, *E–G*). Na_VRosD T207G showed only a small and fast inactivated current (~200 pA; $\tau_{inactivation} < 2$ ms). Because HEK293 or CHO-K1 cells express endogenous sodium channels that produce similar small currents (36), the current produced by the Na_VRosD T207G mutant could not be distinguished from that produced by the endogenous sodium channels. Ala^{226} of Na_VSheP is the residue in the region in the lower part of helix S6 that corresponds to the P*X*P motif in voltage-dependent potassium channels (*green arrow* in Fig. 5*A*). The inactivation rate of Na_VSheP A226G ($\tau_{inactivation}$ = 11.6 ± 0.50 ms at −10 mV) was slightly slower than that of the wild-type channel, but the difference is not statistically significant (Fig. 5*F*). Double mutation of two residues also retained the inward current of sodium ions. The inactivation rate of Na_VBacL A214G/G224A ($\tau_{inactivation}$ = 54.1 ± 4.51 ms at +10 mV, n = 9) was significantly faster than that of Na_VBacL G224A ($p < 0.01$) and slower than that of Na_VBacL A214G, although the difference was not statistically significant (Fig. 5*E*). Na_VSheP A216G/A226G ($\tau_{inactivation}$ = 7.61 ± 0.65 ms at −10 mV) inactivated as fast as Na_VSheP A216G. Na_VRosD T207G/G217A ($\tau_{inactivation}$ = 20.93 ± 3.90 ms at +20 mV) produced a current less than 500 pA. This current could be distinguished from that of endogenous sodium channels and showed a faster inactivation than Na_VRosD G217A ($p < 0.01$). In summary, mutations of the residues corresponding to the glycine hinge accelerated the inactivation rate, mutations of glycines in the lower part of helix S6 to alanine reduced the inactivation rate, and the A226G mutation in Na_VSheP had no effect on the inactivation rate.

DISCUSSION

We cloned three new NaChBac homologues from *B. licheniformis*, *S. putrefaciens*, and *R. denitrificans*. The three channels differ in their kinetics and voltage dependences, which may reflect differences in the environment in which the respective bacteria live. The physiological role of the Na_V homologue found in the alkaliphilic bacterium *Bacillus pseudofirmus*, Na_VBP, has been well studied (6, 12). Deletion of Na_VBP resulted in impaired pH homeostasis and reversed pH chemotaxis (6). These results suggest that Na_VBP functions in conjunction with the multiple resistance and pH adaptation Na^+/H^+ antiporter in pH homeostasis, with the sodium-driven motor protein complex in motility (6), and with the methyl-accepting chemotaxis

TABLE 2

Time constants of activation and inactivation of prokaryotic Na_Vs

The time constant of activation ($\tau_{activation}$) is the time from 10 to 90% of peak current. The time constant of inactivation ($\tau_{inactivation}$) is the time from peak current to 1/e of peak current. All results are expressed as mean ± S.E. The statistical significance of differences in $\tau_{inactivation}$ of each mutant compared to wild-type protein or other mutants is shown in the column, "Statistical significance of $\tau_{inactivation}$." $\tau_{activation}$ and $\tau_{inactivation}$ of NaChBac, Na_VBacL, Na_VSheP, and Na_VRosD were measured at +10, +10, −10, and +20 mV, respectively. All experiments were performed at pH 7.4. To assess statistical differences in $\tau_{inactivation}$ between wild type and mutant proteins, multiple comparisons were made by one-way analysis of variance followed by the Tukey-Kramer multiple comparisons test. NS, not significant.

	Time constant		Statistical significance of $\tau_{inactivation}$			No. of measurements
	$\tau_{activation}$	$\tau_{inactivation}$	WT	G219A	G229A	
	ms					
NaChBac	3.73 ± 0.73	118 ± 10.2				13
NaChBac G219A	0.95 ± 0.22	21.4 ± 2.19	$p < 0.01$			5
NaChBac G229A	12.0 ± 3.33	230 ± 33.8	$p < 0.01$	$p < 0.01$		5
NaChBac G219A/G229A	2.86 ± 0.47	156 ± 16.2	NS	$p < 0.01$	$p < 0.05$	11
			WT	A214G	G224A	
Na_VBacL	4.92 ± 0.73	96.1 ± 9.60				15
Na_VBacL A214G	1.70 ± 0.27	29.5 ± 3.14	$p < 0.01$			11
Na_VBacL G224A	3.69 ± 1.21	270 ± 53.3	$p < 0.01$	$p < 0.01$		5
Na_VBacL A214G/G224A	4.63 ± 0.57	54.1 ± 4.51	NS	NS	$p < 0.01$	9
Na_VBacL G201A	2.20 ± 0.32	81.0 ± 12.6	NS[a]			7
			WT	A216G	G226A	
Na_VSheP	0.89 ± 0.076	9.90 ± 0.57				17
Na_VSheP A216G	0.82 ± 0.10	5.35 ± 0.72	$p < 0.01$			8
Na_VSheP A226G	0.85 ± 0.08	11.6 ± 0.50	NS	$p < 0.01$		9
Na_VSheP A216G/A226G	0.87 ± 0.10	7.61 ± 0.65	$p < 0.05$	NS	$p < 0.01$	10
			WT	G217A		
Na_VRosD	1.61 ± 0.12	9.88 ± 1.25				15
Na_VRosD G217A	2.06 ± 0.45	60.9 ± 13.0	$p < 0.01$			7
Na_VRosD T207G/G217A	2.92 ± 0.63	20.93 ± 3.90	NS	$p < 0.01$		6

[a] A simple comparison between Na_VBacL wild type and G201A was made by Student's *t* test.

proteins in chemotaxis (12). Multiple resistance and pH adaptation antiporters (37), sodium-driven motor protein complex (38), and methyl-accepting chemotaxis proteins (39) are found in many bacteria, and prokaryotic Na_Vs might thus play the same roles in other bacteria as Na_VBP in *B. pseudofirmus*.

Because bacteria live in environments that differ in pH, temperature, and ionic conditions, it seems reasonable that they express Na_Vs with channel properties that have adapted to their specific environments. First, activation and inactivation of prokaryotic Na_Vs cloned from marine bacteria (Na_VSP, Na_VSheP, and Na_VRosD but not Na_VPZ) were faster than those of homologues cloned from *Bacillus* species (NaChBac, Na_VBP, and Na_VBacL) (Table 2). Marine bacteria live in an environment with a higher concentration of sodium ions than soil bacteria, such as *Bacillus* species. The fast inactivation of Na_Vs found in marine bacteria might thus be an adaptation that evolved to prevent the influx of excess sodium ions into the cytoplasm. Second, although Na_VBacL and Na_VBP, both expressed in *Bacillus* species isolated from soil, have similar kinetics of activation and inactivation, their voltage dependences differ from each other. At the neutral pH of 7.4, half of Na_VBP is activated by a voltage of −35 mV and inactivated by a voltage of −57 mV (6) (Table 1). These membrane potentials are 30 mV higher than those that activate and inactivate Na_VBacL. At pH 9.0, the pH of the environment in which *B. pseudofirmus* lives, half of Na_VBP is, however, activated by a voltage of −64 mV and inactivated by a voltage of −86 mV (6). Hence, at the pH of the environment in which the respective bacterium lives, the two channels have similar voltage dependences of activation and inactivation. This finding suggests that the channel characteristics of prokaryotic Na_Vs have been optimized for the specific environments of the bacteria.

The diversity in the channel properties of prokaryotic Na_Vs can help us to obtain a better understanding of the molecular mechanisms that underlie ion channel function. The crystal structure of the $K_V1.2/K_V2.1$ chimera potassium channel suggested that the S4-S5 linker helix pushes down on the lower part of helix S6 and thus keeps the ion pore closed in the resting state (13). A single molecule study demonstrated that this region of KcsA is rotated in the open state (40) and thus confirmed that this region works as an activation gate. If the pore domain were folded tightly, such as seen in crystal structures of potassium channels, the role of the glycine hinge and the P*X*P motif in channel gating might be to provide sufficient flexibility to allow the lower part of helix S6 to bend and move for activation. On the other hand, prokaryotic Na_V mutants lacking glycine and proline residues in helix S6 and wild-type Na_VSheP still show activation and inactivation (Fig. 5 and Table 2). Neither motif can thus be essential for gating in prokaryotic Na_Vs. Because bending of helix S6 would be difficult without such gating motifs, it is likely that in these mutants and in wild-type Na_VSheP, the entire helix S6 has to incline to open the activation gate. Therefore, it is likely that the pore domain of prokaryotic Na_Vs is folded more loosely to increase the mobility of helix S6.

Inactivation of prokaryotic Na_Vs is thought to occur through the C-type inactivation mechanism seen in other tetrameric cation channels. C-type inactivation has been explained by conformational changes around the selectivity filter of the channel (23–25). These conformational changes, which cause the selectivity filter to collapse, act as an inactivation gate. Therefore, the stability of the selectivity filter could affect the rate of C-type inactivation. In the case of KcsA, it has been proposed that the residues adjacent to Gly^{99}, which is the residue corresponding to the glycine hinge, interact with residues forming the bottom

of the selectivity filter, thus stabilizing its conductive conformation (41). This motif of K_v1.2 also locates beside the selectivity filter (Fig. 5, *B* and *C*). Based on the similarity of the primary sequences, the corresponding region in prokaryotic Na_Vs would also be near their selectivity filters. All mutations in this region in Na_VBacL (A214G), Na_VSheP (A216G), Na_VRosD (T207G), and also NaChBac (G219A) accelerated the inactivation rate. Remarkably, the T207G mutation reduced ion currents in Na_VRosD T207G and Na_VRosD T207G/G217A. These mutations would be expected to make the selectivity filter less stable and easier to collapse. As a result, the mutants would inactivate faster than the respective wild-type channels.

The lower part of helix S6 is thought to act as activation gate (13, 40). C-type inactivation always occurs after activation and thus appears to be coupled to activation. The coupling between the activation and inactivation gates is thought to be mediated by residues adjacent to the glycine hinge in helix S6 and the bottom of the selectivity filter (41). Our glycine-to-alanine mutations in the lower part of helix S6 reduced the inactivation rate. This result suggests that the glycine-to-alanine mutations, which stabilize the lower part of helix S6, weaken the coupling between the activation and inactivation gates and thus delay inactivation. Na_VSheP is the only channel in which the alanine-to-glycine mutation (A226G) showed no effect. It thus appears that although this region is important for the coupling in other channels, it may not have the same importance for coupling in Na_VSheP. This notion is supported by the fact that Na_VSheP lacks glycines in helix S6 and may thus use a coupling mechanism that in its details differs from that of other prokaryotic Na_Vs. In a previous report, a G219P mutation in NaChBac eliminated C-type inactivation (16). However, this glycine residue is not obligatory for activation gating. Therefore, the G219P mutation might force helix S6 to adopt an unusual bent conformation, in which helix S6 would not be able to mediate the coupling between the activation and inactivation gates.

Double mutations in the region corresponding to the glycine hinge and the lower part of helix S6 independently affected the inactivation rate in Na_VBacL, Na_VRosD, and NaChBac. It is possible that other regions in helix S6 are also involved in C-type inactivation. Nevertheless, the mutational results at these two regions may serve as useful footholds for the study of C-type inactivation. All mutations in this study had stronger effects on the inactivation rate than on the activation rate. The driving force for activation is depolarization, whereas C-type inactivation is due to the collapse of the selectivity filter, which depends on thermal instability. It is thus not unexpected that C-type inactivation is more sensitive to mutations than channel activation. Although these results provide first clues to the coupling of activation and inactivation in voltage-gated cation channels, a deep understanding of this phenomenon will require further mutational studies as well as the analysis of atomic structures.

Without knowing the three-dimensional structure of Na_V channels, it is impossible to understand the sodium selectivity of these channels and how small changes in their primary sequences result in different voltage dependences and gating kinetics. A high resolution structure is particularly crucial for understanding the structural basis of sodium selectivity. Because the three Na_Vs characterized in this study could be expressed at high levels and purified in large amounts, they are promising candidates for structural studies and thus increase the chances of obtaining a high resolution crystal structure.

Prokaryotic Na_Vs are the simplest voltage-gated cation channels known to date. They are composed of fewer than 300 amino acids, and differences in their channel characteristics are due to small changes in their primary sequences. As functional analyses proceed and structures become available, prokaryotic Na_Vs have the potential not only to reveal the basic molecular mechanisms of voltage-gated cation channels but also to provide insight into the molecular evolution of these channels.

Acknowledgments—We thank Dr. Chikara Sato (Advanced Industrial Science and Technology, Neuroscience Research Institute) for kindly providing NaChBac DNA and Drs. Christoph Gerle and Kentaro Noma for valuable discussions. We are grateful to Dr. Thomas Walz for critical reading of the manuscript.

REFERENCES

1. Hille, B. (2001) *Ion Channels of Excitable Membranes*, 3rd Ed., Sinauer Associates, Sunderland, MA
2. Catterall, W. A. (1992) *Physiol. Rev.* **72,** S15–S48
3. Catterall, W. A. (1995) *Annu. Rev. Biochem.* **64,** 493–531
4. Sato, C., Ueno, Y., Asai, K., Takahashi, K., Sato, M., Engel, A., and Fujiyoshi, Y. (2001) *Nature* **409,** 1047–1051
5. Ren, D., Navarro, B., Xu, H., Yue, L., Shi, Q., and Clapham, D. E. (2001) *Science* **294,** 2372–2375
6. Ito, M., Xu, H., Guffanti, A. A., Wei, Y., Zvi, L., Clapham, D. E., and Krulwich, T. A. (2004) *Proc. Natl. Acad. Sci. U.S.A.* **101,** 10566–10571
7. Koishi, R., Xu, H., Ren, D., Navarro, B., Spiller, B. W., Shi, Q., and Clapham, D. E. (2004) *J. Biol. Chem.* **279,** 9532–9538
8. Doyle, D. A., Morais Cabral, J., Pfuetzner, R. A., Kuo, A., Gulbis, J. M., Cohen, S. L., Chait, B. T., and MacKinnon, R. (1998) *Science* **280,** 69–77
9. Jiang, Y., Lee, A., Chen, J., Ruta, V., Cadene, M., Chait, B. T., and MacKinnon, R. (2003) *Nature* **423,** 33–41
10. Jiang, Y., Lee, A., Chen, J., Cadene, M., Chait, B. T., and MacKinnon, R. (2002) *Nature* **417,** 515–522
11. Nurani, G., Radford, M., Charalambous, K., O'Reilly, A. O., Cronin, N. B., Haque, S., and Wallace, B. A. (2008) *Biochemistry* **47,** 8114–8121
12. Fujinami, S., Sato, T., Trimmer, J. S., Spiller, B. W., Clapham, D. E., Krulwich, T. A., Kawagishi, I., and Ito, M. (2007) *Microbiology* **153,** 4027–4038
13. Long, S. B., Tao, X., Campbell, E. B., and MacKinnon, R. (2007) *Nature* **450,** 376–382
14. Alam, A., and Jiang, Y. (2009) *Nat. Struct. Mol. Biol.* **16,** 30–34
15. Jiang, Y., Lee, A., Chen, J., Cadene, M., Chait, B. T., and MacKinnon, R. (2002) *Nature* **417,** 523–526
16. Zhao, Y., Yarov-Yarovoy, V., Scheuer, T., and Catterall, W. A. (2004) *Neuron* **41,** 859–865
17. Ding, S., Ingleby, L., Ahern, C. A., and Horn, R. (2005) *J. Gen. Physiol.* **126,** 213–226
18. Hardman, R. M., Stansfeld, P. J., Dalibalta, S., Sutcliffe, M. J., and Mitcheson, J. S. (2007) *J. Biol. Chem.* **282,** 31972–31981
19. Labro, A. J., Raes, A. L., Bellens, I., Ottschytsch, N., and Snyders, D. J. (2003) *J. Biol. Chem.* **278,** 50724–50731
20. Armstrong, C. M., and Bezanilla, F. (1977) *J. Gen. Physiol.* **70,** 567–590
21. Murrell-Lagnado, R. D., and Aldrich, R. W. (1993) *J. Gen. Physiol.* **102,** 949–975
22. Murrell-Lagnado, R. D., and Aldrich, R. W. (1993) *J. Gen. Physiol.* **102,** 977–1003
23. Ogielska, E. M., Zagotta, W. N., Hoshi, T., Heinemann, S. H., Haab, J., and Aldrich, R. W. (1995) *Biophys. J.* **69,** 2449–2457
24. Ong, B. H., Tomaselli, G. F., and Balser, J. R. (2000) *J. Gen. Physiol.* **116,**

653–662
25. Pavlov, E., Bladen, C., Winkfein, R., Diao, C., Dhaliwal, P., and French, R. J. (2005) *Biophys. J.* **89,** 232–242
26. Blunck, R., Starace, D. M., Correa, A. M., and Bezanilla, F. (2004) *Biophys. J.* **86,** 3966–3980
27. Rey, M. W., Ramaiya, P., Nelson, B. A., Brody-Karpin, S. D., Zaretsky, E. J., Tang, M., Lopez de Leon, A., Xiang, H., Gusti, V., Clausen, I. G., Olsen, P. B., Rasmussen, M. D., Andersen, J. T., Jørgensen, P. L., Larsen, T. S., Sorokin, A., Bolotin, A., Lapidus, A., Galleron, N., Ehrlich, S. D., and Berka, R. M. (2004) *Genome Biol.* **5,** R77
28. Van Trappen, S., Mergaert, J., and Swings, J. (2004) *Int. J. Syst. Evol. Microbiol.* **54,** 1263–1269
29. Choudhary, M., Zanhua, X., Fu, Y. X., and Kaplan, S. (2007) *J. Bacteriol.* **189,** 1914–1921
30. Ziemke, F., Höfle, M. G., Lalucat, J., and Rosselló-Mora, R. (1998) *Int. J. Syst. Bacteriol.* **48,** 179–186
31. Swingley, W. D., Sadekar, S., Mastrian, S. D., Matthies, H. J., Hao, J., Ramos, H., Acharya, C. R., Conrad, A. L., Taylor, H. L., Dejesa, L. C., Shah, M. K., O'huallachain, M. E., Lince, M. T., Blankenship, R. E., Beatty, J. T., and Touchman, J. W. (2007) *J. Bacteriol.* **189,** 683–690
32. Strömpl, C., Hold, G. L., Lünsdorf, H., Graham, J., Gallacher, S., Abraham, W. R., Moore, E. R., and Timmis, K. N. (2003) *Int. J. Syst. Evol. Microbiol.* **53,** 1901–1906
33. Hümbelin, M., Thomas, A., Lin, J., Li, J., Jore, J., and Berry, A. (2002) *Gene* **297,** 129–139
34. Patton, D. E., Isom, L. L., Catterall, W. A., and Goldin, A. L. (1994) *J. Biol. Chem.* **269,** 17649–17655
35. O'Neil, K. T., and DeGrado, W. F. (1990) *Science* **250,** 646–651
36. Lalik, P. H., Krafte, D. S., Volberg, W. A., and Ciccarelli, R. B. (1993) *Am. J. Physiol.* **264,** C803–C809
37. Swartz, T. H., Ikewada, S., Ishikawa, O., Ito, M., and Krulwich, T. A. (2005) *Extremophiles* **9,** 345–354
38. Ito, M., Hicks, D. B., Henkin, T. M., Guffanti, A. A., Powers, B. D., Zvi, L., Uematsu, K., and Krulwich, T. A. (2004) *Mol. Microbiol.* **53,** 1035–1049
39. McEvoy, M. M., and Dahlquist, F. W. (1997) *Curr. Opin. Struct. Biol.* **7,** 793–797
40. Shimizu, H., Iwamoto, M., Konno, T., Nihei, A., Sasaki, Y. C., and Oiki, S. (2008) *Cell* **132,** 67–78
41. Blunck, R., Cordero-Morales, J. F., Cuello, L. G., Perozo, E., and Bezanilla, F. (2006) *J. Gen. Physiol.* **128,** 569–581